Surface State Spectrum of AlGaN/AlN/GaN Extracted from Static Equilibrium Electrostatics

Hao Yu, *Member, IEEE,* Alireza Alian, Uthayasankaran Peralagu, Ming Zhao, Niamh Waldron, Bertrand Parvais, and Nadine Collaert

***Abstract*—We extract an AlGaN surface state spectrum with a density (D_{SS}) ranging between 1.4×10^{12} and 4.7×10^{12} $eV^{-1}cm^{-2}$. The low D_{SS} is achieved with *in-situ* SiN passivation. The D_{SS} are extracted from ungated AlGaN/AlN/GaN heterostructures with varied AlN thicknesses between 0 to 2nm: Increased AlN thicknesses in heterostructures monotonously increase 2DEG densities N_{sh} and AlGaN surface potential energies $q\varphi_s$, and the D_{SS} is extracted with ΔN_{sh}-$\Delta\varphi_s$ correlations. The D_{SS} extraction methodology in this work features calibrated polarization charge values, Hartree approximation based 2DEG profile calculation, and incorporated C-GaN substrate impact on 2DEG. We also extract the charge neutrality level at the AlGaN surface, which is ~0.95 eV below conduction band minimum.**

***Index Terms*—AlGaN surface state, III-N HEMT, polarization charge, 2DEG quantum well,**

I. Introduction

AlGaN/GaN high electron mobility transistors (HEMTs) featuring a high current density and a high breakdown voltage are promising candidate devices in power electronics and 5G/6G RF applications [1]–[4]. High AlGaN surface state density (D_{SS}, in $eV^{-1}cm^{-2}$) has been a major problem that compromises efficiency of AlGaN/GaN HEMTs. High D_{SS} causes current collapses [5], induces high gate leakage [6], and reduces breakdown voltage [7] of HEMTs. To reduce the AlGaN D_{SS}, passivation solutions have been explored [8]–[10].

Quantitative evaluation of AlGaN surface passivation solutions relies on accurate measurement of the D_{SS}. D_{SS} characterization methods are multiple, but they can be simply categorized into dynamic and static methods depending on usage of bias voltages. In dynamic methods, multiple bias voltages—direct current (dc) or alternating current (ac) signals—are applied on metal/insulator/AlGaN/GaN MIS capacitors or MIS-HEMT devices, and the D_{SS} is extracted from surface state capture/emission responses. The accuracy of dynamic methods is challenged by correct determination of the steady state response and of the equivalent circuit of the test structures. This challenge is especially problematic for III-N heterostructures because of their multiple barriers/interfaces and usual lack of fast-responding dopants. In contrast, in static equilibrium methods for D_{SS} extraction, near-zero biases are applied, and the electrostatics of heterostructures thus remain unvaried. In these methods, ungated heterostructures are fabricated with multiple AlGaN (or InAlN) barrier or AlN interlayer (IL) thicknesses, and the D_{SS} is extracted by correlating variations of 2DEG sheet densities (N_{sh}, in cm^{-2}) with those of barrier surface potential energies ($q\varphi_S$, q is elementary charge) [11]–[17]. The static methods are based on electrostatics at rigorously equilibrium states; the surface states within $q\varphi_S$ intervals are thoroughly counted. So far, the D_{SS} reported with static methods are generally high [11]–[17]: the lowest reported D_{SS} of the AlGaN is 4.6×10^{12} $eV^{-1}cm^{-2}$ in [13] with optimized surface etching [12].

Accurate calculation of the electrostatics of heterostructures is crucial to static methods. In this work, we demonstrate a fully analytical static method featuring (a) Hartree approximation based 2DEG profile calculation, (b) inclusion of the substrate impact on the N_{sh}, and (c) experimental calibration of polarization charges (σ, in C/cm^2) of the heterostructure interfaces. We extract a low-D_{SS} spectrum with an average magnitude of ~2.9×10^{12} $eV^{-1}cm^{-2}$, demonstrating successful AlGaN surface passivation by an *in-situ* SiN. To our knowledge, the D_{SS} is the lowest compared to past studies using static methods [11]–[17]. Also, it is the first time that a surface state spectrum is extracted using a static method, attributed to consistent φ_S-N_{sh} correlations among the heterostructures in this study. In addition, we extract the charge neutrality level of the SiN passivated AlGaN surface, which is ~0.95 eV below AlGaN conduction band E_C minimum.

II. Experimental

Epitaxial structures were grown by MOCVD on high-resistivity 200 mm Si (111) substrates using the method in [18], [19]. A schematic of top layers of samples in this work is shown in Fig. 1a. 300 nm undoped GaN (i-GaN) was grown on a thick C doped GaN layer (C-GaN) [20]. The fully relaxed i-GaN provides a template for pseudomorphic growth of the AlGaN/AlN layers. Two sets of samples with varied epitaxial AlN/$Al_{0.25}Ga_{0.75}N$ thicknesses were prepared: one set is composed of a 0, 0.5, 1, 1.5, or 2 nm AlN IL and a 15 nm AlGaN barrier; the other set of a 1 nm AlN and a 4, 10, or 15 nm AlGaN. The AlN/AlGaN layers were undoped. The AlGaN surfaces of all samples were passivated with in-situ SiN [21].

Manuscript submitted July 6, 2021. This work was supported by imec's advanced RF program (Corresponding authors: Hao Yu).

Hao Yu, Alian Alireza, Uthayasankaran Peralagu, Ming Zhao, and Nadine Collaert are with imec, 3001 Leuven, Belgium. (e-mail: hao.yu@imec.be).

Niamh Waldron was with imec, 3001 Leuven, Belgium, and now with Facebook, Cork, County Cork, Ireland.

Bertrand Parvais is with imec, 3001 Leuven, Belgium, and also with Vrije Universiteit Brussel, Brussels, Belgium.

confidential

The in-situ SiN growth method has been introduced in [22]. 250×250 μm^2 square Van der Pauw (VDP) structures were fabricated for measurement of 2DEG N_{sh} and sheet resistances (R_{sh}). The N_{sh} was obtained from Hall effect measurements of VDP structures. HEMTs with 1 μm gate length and 10 μm width were fabricated for threshold voltage (V_{th}) measurement. In the gate region of HEMTs, the SiN layer was etched, and TiN was deposited on AlGaN as the gate metal [21]. V_{th} of HEMTs was extracted with the linear extrapolation method [23] with a 0.1 V drain-to-source voltage.

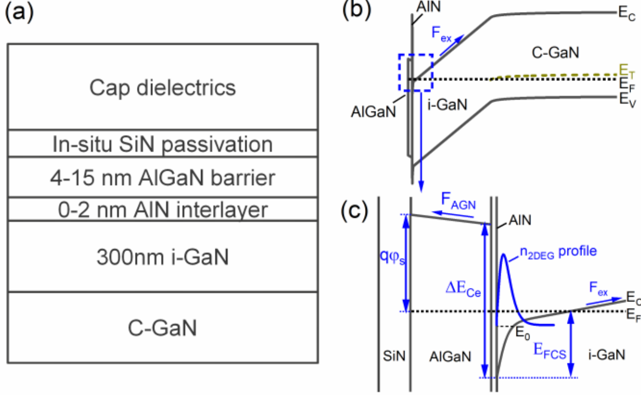

Fig. 1 (a) Schematic layer information of the heterostructure near GaN surface. (b) Schematic energy band diagram of AlGaN/AlN/i-GaN/C-GaN. (c) Zoom of the region near GaN surface with simulated 2DEG concentration n_{2DEG} distribution.

III. Results, Modeling, and Discussion

The 2DEG R_{sh} and N_{sh} as functions of the AlN IL thickness (t_{AN}) and the AlGaN barrier thickness (t_{AGN}) are shown in Fig. 2. In Fig. 2a, we observe that the N_{sh} increases monotonously with the t_{AN}, but the R_{sh} reaches the lowest with a t_{AN} of 0.5 nm or 1 nm. A thin AlN IL is known to push 2DEG centroid away from the AlGaN/GaN interface and reduces interface scattering and AlGaN alloy disorder scattering of the 2DEG [24]. This should improve the 2DEG mobility. As for the degraded 2DEG mobility with the 1.5 nm or 2 nm AlN IL, it may result from increased scattering from the AlN/GaN interface roughness or misfit dislocations in the AlN/AlGaN. Because the tensile stress built within the AlN/AlGaN on a relaxed GaN substrate increases with their thicknesses. Our activities are still ongoing to fully understand the mechanism behind the 2DEG mobility of various heterostructures. Note that all $Al_xGa_{1-x}N$ layers in this work are still below their critical thicknesses of strain relaxation [25]. In later discussion, we will also show how the strain status of the AlGaN and the AlN is examined with V_{th}-$t_{A(G)N}$ curves.

We apply the N_{sh}-t_{AN} and N_{sh}-t_{AGN} dependences to this AlGaN surface state study. Spontaneous polarization charge values (P_{AGN}^{SP}) at c-plane surfaces of wurtzite $Al_xGa_{1-x}N$ increase with Al content x [26], [27]. On relaxed GaN substrates, the tensile strain induced by lattice mismatch creates additional piezoelectric charges in the $Al_xGa_{1-x}N$ (P_{AGN}^{PZ}), which also increases with x. Due to a much higher total polarization charge of σ_{AN} in the AlN IL ($\sigma_{AN} = P_{AN}^{SP} + P_{AN}^{PZ}$) than the σ_{AGN} in the $Al_{0.25}Ga_{0.75}N$ barrier, the AlN IL increases the effective conduction band offset ΔE_{Ce} between AlGaN and GaN [24]. As a result, the AlN IL induces a positive shift of the AlGaN surface potential energy $q\Delta\varphi_S$. The positive $q\Delta\varphi_S$ makes the net surface state charge (qN_{SS}, in C/cm^2) more positive, resulting in increased N_{sh} of 2DEG to maintain charge neutrality. This means that, among samples with varied AlN IL thicknesses t_{AN}, variations of N_{SS} and N_{sh} compensate each other

$$\Delta N_{SS} = \Delta N_{sh} \tag{1}$$

The averaged D_{SS} in each $q\Delta\varphi_S$ is then

$$D_{SS} = \frac{\Delta N_{SS}}{q\Delta\varphi_S} = \frac{\Delta N_{sh}}{q\Delta\varphi_S} \tag{2}$$

The ΔN_{sh} caused by t_{AN} variations are derived from Hall effect measurements in Fig. 2a. The remaining task for D_{SS} extraction with (2) is accurate calculation of $\Delta\varphi_S$, which is explained hereafter.

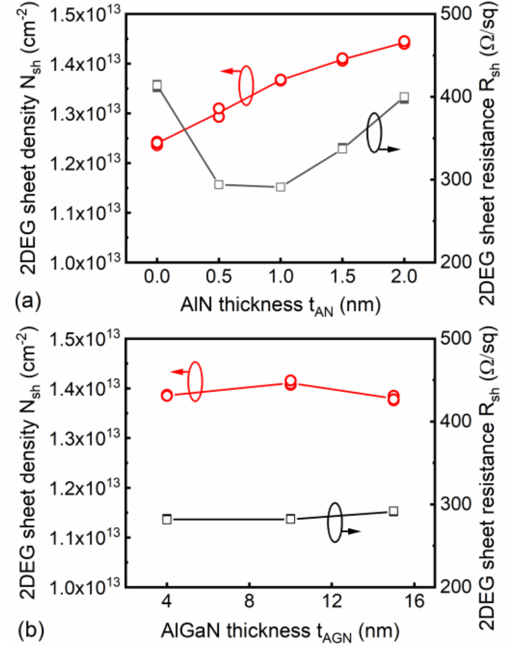

Fig. 2 2DEG N_{sh} and R_{sh} with varied (a) t_{AN} and (b) t_{AGN} in the heterostructure. The heterostructures in (a) with the same 15 nm AlGaN; the samples in (b) with the same 1nm AlN.

As the schematics illustrated in Fig. 1c, fundamentally, calculation of the φ_S requires knowledge of (a) the N_{sh}, (b) the quantum well potential profile at GaN surface, and (c) the σ at heterostructures interfaces. The quantum well potential profile is required to establish the boundary potential energy for the AlGaN/AlN, while the N_{sh} and the σ are required to calculate electric fields across the AlGaN/AlN. The N_{sh} is obtained experimentally in Fig. 2. Next, we make particular efforts in improving accuracy of factors (b) and (c) compared to previous works [11]–[17].

We adopt the Hartree method to calculate the quantum well potential profile [28]. The Hartree approximation is advantageous over triangular well approximation by correctly considering electron-electron interaction in many-electron systems [28]. In the Hartree method, the impact of the external field F_{ex} on N_{sh} can be analytically incorporated [29]. As illustrated in Fig. 1b, the F_{ex} is built between the 2DEG quantum well edge and the C-GaN: in the degenerate quantum well at the i-GaN surface, the Fermi level E_F is above conduction band E_C; in the C-GaN, the E_F is pinned in the lower half of band gap by ionized C acceptors [20]; a constant F_{ex} is thereby built in the undoped i-GaN layer. In the following analytical calculation for the quantum well potential profile, the electron-electron

confidential

interaction induced Hartree potential [28] and the F_{ex} induced external potential are both included.

As shown in Fig. 1c, E_{FCS} is the boundary potential energy at the GaN surface between the E_F and the E_C. In a 2DEG quantum well, the N_{sh} has the following dependence on the E_{FCS} [28]

$$N_{sh} = D_{GN} kT \, ln \left[1 + \exp\left(\frac{E_{FCS} - E_0}{kT}\right)\right] \tag{3}$$

where k is the Boltzmann constant, T is temperature, E_0 is the energy of the first sub-band in a quantum well with respect to E_C, and D_{GN} is the 2D density of states (DOS) in a GaN quantum well

$$D_{GN} = C \frac{m^*_{GN}}{\pi \hbar^2} \tag{4}$$

where $\hbar$ is the reduced Planck constant, m^*_{GN} is the electron density of states effective mass in the E_C of GaN, and C=1.1 is a correction factor for the DOS. C is introduced because only the first sub-band is considered in the Hartree approximation [28]. By simulating an AlGaN/AlN/GaN heterostructure with a 1D Poisson-Schrodinger solver [30], we note that 88%~91% of the 2DEG is occupied by the first sub-band in the GaN quantum well when the N_{sh} varies between 3×10^{12} and 2×10^{13} cm^{-2}. Therefore, the first sub-band is dominant, but neglecting the second and other upper sub-bands causes underestimation of DOS by ~10%. C=1.1 is thus introduced in (4) to compensate the DOS underestimation in the Hartree method.

Then we incorporate the F_{ex} impact on the GaN surface quantum well into the Hartree approximation method [28]

$$E_0 = \frac{3}{2}\left[\frac{(\hbar c)^2}{4m^*}\right]^{1/3} + \frac{c - 3qF_{ex}}{b} \tag{5}$$

where b and c are two intermediate variables

$$c = 3qF_{ex} + \frac{33q^2 N_{sh}}{32\varepsilon} \tag{6}$$

$$b = \left(\frac{4cm^*}{\hbar^2}\right)^{1/3} \tag{7}$$

With knowledge of the N_{sh} and the F_{ex}, (3)-(7) help derive the boundary E_{FCS} and the sub-band level E_0. The distribution of the 2DEG in a quantum well follows the normalized Fang—Howard wave function [28]

$$\psi(x) = \frac{b^{3/2}}{\sqrt{2}} x \exp\left(-\frac{1}{2}bx\right) \tag{8}$$

As illustrated in the schematics Fig. 1c, after deriving the E_{FCS}, the φ_S is simply

$$\varphi_S = (\Delta E_{Ce} - E_{FCS})/q + F_{AGN} t_{AGN} \tag{9}$$

where F_{AGN} is the electric field across the AlGaN (direction see Fig. 1c)

$$F_{AGN} = \frac{\sigma_{AGN} - \sigma_{GN} - qN_{sh}}{\varepsilon} - F_{ex} \tag{10}$$

and ΔE_{Ce} is the effective conduction band offset ΔE_{Ce} between the AlGaN and the GaN, which increases with the AlN thickness t_{AN}

$$\begin{aligned} \Delta E_{Ce} &= \Delta\chi_e + qF_{AN} t_{AN} \\ &= \Delta\chi_e + q\left(\frac{\sigma_{AN} - \sigma_{GN} - qN_{sh}}{\varepsilon} - F_{ex}\right) t_{AN} \end{aligned} \tag{11}$$

where F_{AN} is the electric field across the AlN, ε is the dielectric constant of wurtzite $Al_xGa_{1-x}N$ (ε is almost the same for 0≤x≤1), σ_{GN} is the (spontaneous) polarization charge of GaN, and $\Delta\chi_e$ is the constant difference of the electron affinity between $Al_{0.25}Ga_{0.75}N$ and GaN [31].

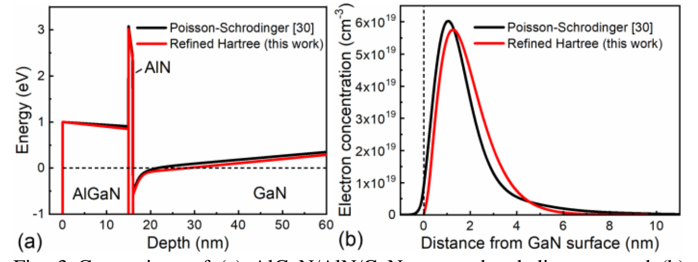

Fig. 3 Comparison of (a) AlGaN/AlN/GaN energy band diagrams and (b) electron concentration distribution simulated by a Poisson-Schrodinger solver [30] and by the refined analytical Hartree method in this work. The same material parameters including a fixed φ_S of 1.0 eV are put in the two simulations. The simulated N_{sh} differences between the two methods remain lower than 1% when φ_S varies between 0.5 eV to 5 eV.

The analytical formula set (3)-(11) describes how a III-N heterostructure is simulated by a refined Hartree method. In Fig. 3, we verify resemblance of simulated energy band diagram and electron distribution with the refined Hartree method to those with the Poisson-Schrodinger solver [30]. The agreement is encouraging. The refined Hartree method achieves simple and analytical 2DEG simulation and φ_s calculation, which makes it a promising to be incorporated into future compact modeling.

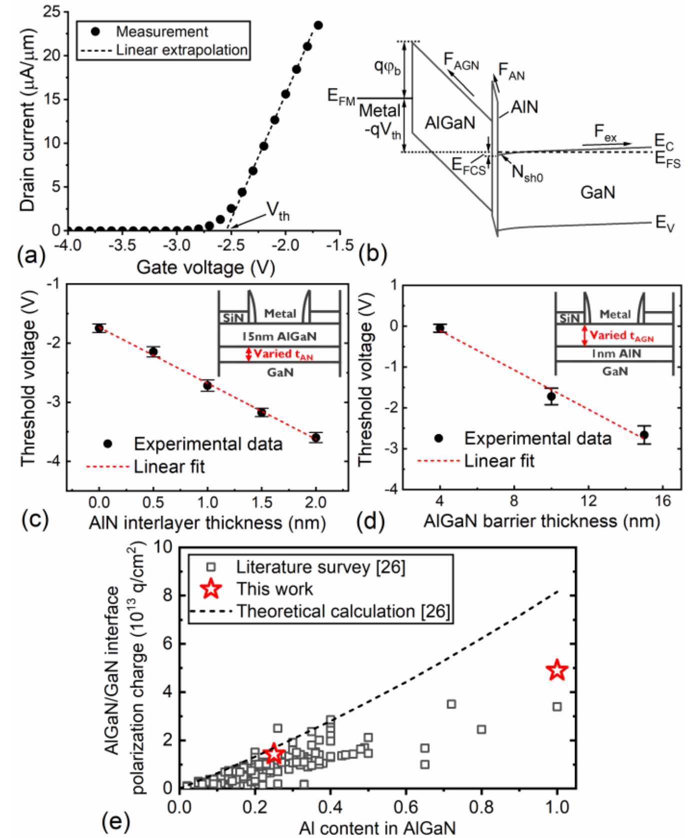

Fig. 4 (a) Illustration of V_{th} extraction from drain current-gate voltage curve at 0.1V drain to source voltage using linear extrapolation method. (b) Schematic of energy band diagram of HEMT gate region at V_{th}. (c) and (d) show V_{th} of HEMT as a function of t_{AN} or t_{AGN} with drain-to-source voltage of 0.1V; Insets show schematic device cross sections. (e) Extracted $\sigma_{AN} - \sigma_{GN}$ and $\sigma_{AGN} - \sigma_{GN}$ are compared to experimental data survey in literature and theoretical prediction by Dreyer *et al.* in [26].

(9)-(11) show how the φ_s depends on the σ. In previous studies [11]–[17], theoretical values of σ were adopted in φ_s calculation. But experimental σ usually deviate from theoretical

confidential

prediction [26], as shown in Fig. 4e. This necessitates applying experimentally calibrated σ into calculation of the φ_S.

We extract the σ_{AN}-σ_{GN} and the σ_{AGN}-σ_{GN} from V_{th}-$t_{A(G)N}$ correlations. As illustrated in Fig. 4a, The V_{th} of HEMTs is extracted with the linear extrapolation method on drain current-gate voltage curves [23]. As illustrated in Fig. 4b, the V_{th} of a HEMT is calculated by

$$V_{th} = \varphi_b - F_{AGN}t_{AGN} - \frac{\Delta E_{Ce}}{q} + E_{FCS}(N_{sh0}) \qquad (12)$$

where φ_b is the gate Schottky barrier height, N_{sh0} is the remaining 2DEG density in the channel of HEMTs at V_{th}, approximately 2×10^{12} cm^{-2}. Taking (10) and (11) into (12), we derive ΔV_{th} vs $\Delta t_{A(G)N}$

$$\begin{aligned}\Delta V_{th} &= -F_{AGN}\Delta t_{AGN} - F_{AN}\Delta t_{AN} \\ &= -\left(\frac{\sigma_{AGN} - \sigma_{GN} - qN_{sh0}}{\varepsilon} - F_{ex}\right)\Delta t_{AGN} \\ &\quad -\left(\frac{\sigma_{AN} - \sigma_{GN} - qN_{sh0}}{\varepsilon} - F_{ex}\right)\Delta t_{AN} \qquad (13)\end{aligned}$$

(13) allows us to extract experimental σ_{AN}-σ_{GN} and σ_{AGN}-σ_{GN} from slopes of curves in Fig. 4c and 4d. The σ_{AN} and σ_{AGN} are lower than theoretical prediction, possibly due to partial strain relaxation of AlN and AlGaN on the GaN substrate. The linearity of the V_{th}-$t_{A(G)N}$ curves in (c) and (d) suggests that the tensile strain built within the AlGaN and the AlN is consistent among all samples. The experimental σ are then fed into (8)-(10) for φ_S calculation.

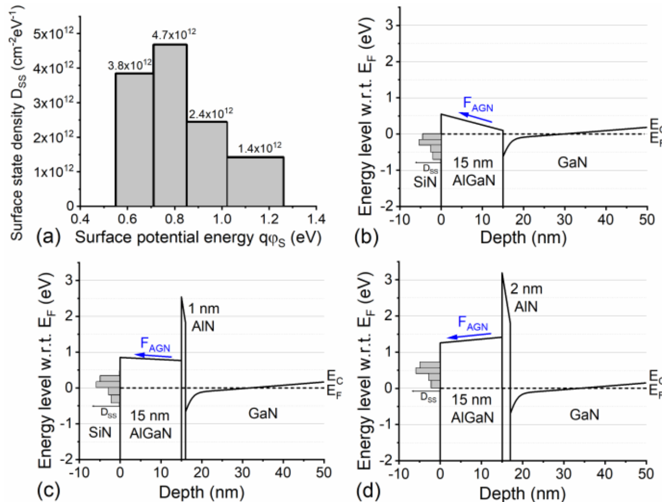

Fig. 5 (a) D_{SS} spectrum of AlGaN surface as a function $q\varphi_S$. Calculated energy band diagram of (b) SiN/15 nm AlGaN/i-GaN/C-GaN, (c) SiN/15 nm AlGaN/1 nm AlN/i-GaN/C-GaN, and (d) SiN/15 nm AlGaN/2 nm AlN/i-GaN/C-GaN with D_{SS} distribution illustrated at AlGaN surface. SiN, part of i-GaN, and C-GaN are not shown in (b)-(d) for simplicity.

The ΔE_{Ce} increases substantially with the t_{AN}, as in (11), making φ_S increase monotonously with t_{AN}. Five t_{AN} splits in this work create four $\Delta\varphi_S$ intervals. The D_{SS} in each $\Delta\varphi_S$ interval is calculated with (2) and shown in Fig. 5a. A D_{SS} spectrum is thus derived with a span of ~0.7eV and magnitudes varying between 1.4×10^{12} and 4.7×10^{12} eV^{-1}cm^{-2}. The D_{SS} magnitudes within the spectrum indicate non-existence of discrete single states that have a surface density above 1×10^{12} cm^{-2}. Besides the D_{SS}, complete energy band diagrams of the AlGaN/AlN/GaN with varied AlGaN/AlN thicknesses are also derived. Examples of the energy band diagrams are shown in Fig. 5b-d.

The energy band diagrams reflect electrostatics of the heterostructures at equilibrium. Interestingly, we can also derive the surface charge neutrality level E_{CNLS} of the AlGaN from the energy band diagrams. The E_{CNLS} is practically defined as following: when the E_F overlaps with the E_{CNLS} at equilibrium, the net charge at the AlGaN surface is zero. The E_{CNLS} of the AlGaN represents a reference position of E_F at which the surface polarization charges are equally compensated by surface state charges. Among the energy band diagrams of Fig. 5b-d, a flip of the F_{AGN} direction is noted when the t_{AN} is varied between 0 nm and 2 nm. It means the polarity of the net surface charge is flipped, or in other words, the E_F sweeps over the E_{CNLS} of the AlGaN. Based on the D_{SS} and the φ_S with varied t_{AN}, E_{CNLS} is estimated to be ~0.95 eV below the E_C minimum of the AlGaN surface. As shown in Fig. 5c, the AlGaN is nearly flat-band with 1nm AlN, corresponding to a condition that the E_F is close to E_{CNLS}. In such conditions, varying AlGaN thicknesses induces little $\Delta\varphi_S$; consequently, the N_{sh} and the R_{sh} of 2DEG vary little with the t_{AGN} in Fig. 2b. Knowledge of the D_{SS} and the E_{CNLS} correlates quantitatively the F_{AGN} with the φ_S by

$$F_{AGN} = -\frac{qD_{SS}(q\varphi_S - E_{CNL})}{\varepsilon} \qquad (14)$$

Extension of the above relationship with (3)-(10) would enable prediction of the N_{sh} with given t_{AGN} and t_{AN} [32].

This work belongs to the D_{SS} extraction methods that make use of static equilibrium electrostatics of ungated heterostructures. In these methods, N_{sh} measurement and φ_S calculation are the basic steps to derive the D_{SS}. Only small longitudinal fields are applied on VDP structures in the N_{sh} measurement, so the electrostatics of the heterostructures remain close to zero-bias conditions. In such near-zero-bias conditions, all defects comply with the same Fermi-Dirac distribution. This avoids complicated determination of the steady state and the equivalent circuit of test structures, which are usually error sources of D_{SS} in methods using dynamic bias voltages. Due to the methodology differences, the following discussion involves only the static equilibrium methods.

The fully analytical D_{SS} extraction methodology in this work features (a) experimentally calibrated σ of heterostructures and (b) Hartree approximation based 2DEG profile calculation. These are advances compared to traditional equilibrium electrostatics based D_{SS} extraction methods [11]–[17]. According to Fig. 4e and the equations (2) and (9)-(11), the use of theoretical σ values would usually result in overestimation of σ, φ_S, and $\Delta\varphi_S$, and eventually underestimation of D_{SS}; the D_{SS} underestimation degree would be approximately the same as that of the σ overestimation. As for the 2DEG profile calculation, we incorporate the substrate impact on 2DEG into the Hartree approximation method. This makes the methodology applicable to various substrates and is especially helpful for those studies with thin i-GaN channel layers.

It is worth noting that the D_{SS} reported with the static equilibrium methods were usually high, as summarized in Table I. This poses serious concerns, as a high D_{SS} of the barrier is a direct cause of degradation and reliability concerns—such as serious current collapses, high gate leakage, and low breakdown voltages—of HEMT or MIS-HEMT devices. In this work, the low D_{SS} of the AlGaN and the high N_{sh} of 2DEG achieved with the *in-situ* SiN passivation are encouraging. It is

aligned with the good dc and RF performance demonstrated with our devices [4], [21]. The *in-situ* SiN reduces relaxation, cracking, and surface roughness of the AlGaN layer [22]. Moreover, it helps avoid AlGaN surface oxidation, which is a major cause of AlGaN surface states [33]. Since the *in-situ* SiN is not only critical for epitaxy engineering but also prevents air exposure of the AlGaN, it is found much superior to *ex-situ* SiN passivation [34].

TABLE I SUMMARY OF D_{SS} STUDIES THAT ARE BASED ON STATIC EQUILIBRIUM ELECTROSTATICS OF III-N HETEROSTRUCTURES

Ref.	Barrier	With AlN IL?	Method	Passivation/ surface treatment	Avg. D_{SS} (10^{12} $eV^{-1}cm^{-2}$)
[11]	$Al_{0.34}Ga_{0.66}N$	No	Vary t_{AGN}	w/o	>11
[13]	$Al_{0.19}Ga_{0.81}N$	No	Vary t_{AGN}	RIE[a]	4.6
[13]	$Al_{0.24}Ga_{0.76}N$	No	Vary t_{AGN}	RIE[a]	6.1
[13]	$Al_{0.29}Ga_{0.71}N$	No	Vary t_{AGN}	RIE[a]	7.5
[14]	$Al_{0.3}Ga_{0.7}N$	No	Vary t_{AGN}	w/o	7.8
[14]	$Al_{0.3}Ga_{0.7}N$	No	Vary t_{AGN}	SiN	17.8
[15]	$Al_{0.3}Ga_{0.7}N$ $Al_{0.35}Ga_{0.65}N$ $Al_{0.4}Ga_{0.6}N$	No	Vary Al% in AlGaN	SiN	18.5
[16]	$In_{0.17}Al_{0.83}N$	Yes	Vary t_{IAN}[b]	N/A	35
[16]	$In_{0.07}Al_{0.93}N$ $In_{0.12}Al_{0.88}N$ $In_{0.145}Al_{0.855}N$	Yes	Vary Al% in InAlN	w/o	16.8
[17]	$In_{0.169}Al_{0.831}N$	No	Vary t_{IAN}	w/o	82.7
[17]	$In_{0.182}Al_{0.818}N$	No	Vary t_{IAN}	w/o	68.1
[17]	$In_{0.098}Al_{0.902}N$	No	Vary t_{IAN}	w/o	46.4
This work	$Al_{0.25}Ga_{0.75}N$	Yes	Vary t_{AN}	*In-situ* SiN	2.9

[a] RIE: Cl-based reactive ion etching [12]
[b] t_{IAN}: InAlN thickness

Knowledge of the D_{SS} is not only important to evaluation of barrier passivation techniques, but also to modeling HEMT or MIS-HEMT. The extracted D_{SS} spectrum and the E_{CNLS} of the AlGaN make solid foundations for future compact modeling development: this includes modeling of access region resistances, gate/drain corner field distribution, gate leakage, current collapses, etc.

IV. CONCLUSIONS

In this work, we investigate surface state densities (D_{SS}) of the AlGaN/AlN/GaN heterostructures passivated by the *in-situ* SiN. We demonstrate a fully analytical D_{SS} extraction method. In the method, we build quantitative correlations between the AlGaN surface states and the static equilibrium electrostatics of heterostructures with varied AlGaN barrier/AlN interlayer thicknesses. We introduce several key advancements that ensure accurate calculation of electrostatics: we apply the Hartree approximation method in quantum well potential profile calculation; we include analytically the C-GaN substrate impact on 2DEG distribution; and we calibrate experimentally polarization charge values of the III-N layers. With the optimized method, we report low D_{SS} varying between 1.4×10^{12} and 4.7×10^{12} $eV^{-1}cm^{-2}$, which proves successful AlGaN passivation with the *in-situ* SiN. Besides the D_{SS}, we also derive the charge neutrality level E_{CNLS} at the AlGaN surface, which is ~0.95 eV below the E_C of the AlGaN. The fully analytical simulation method in this work is promising to be incorporated into future compact modeling, while knowledge of the D_{SS} spectrum and the E_{CNLS} will contribute to accurate trapping modeling in AlGaN/GaN (MIS-)HEMT.

REFERENCES

[1] U. K. Mishra, L. Shen, T. E. Kazior, and Y. F. Wu, "GaN-based RF power devices and amplifiers," *Proc. IEEE*, vol. 96, no. 2, pp. 287–305, 2008, doi: 10.1109/JPROC.2007.911060.

[2] M. Micovic *et al.*, "High frequency GaN HEMTs for RF MMIC applications," in *IEEE International Electron Devices Meeting*, 2016, pp. 59–62, doi: 10.1109/MWSYM.2013.6697656.

[3] N. Collaert *et al.*, "(Plenary) The revival of compound semiconductors and how they will change the world in a 5G/6G era," *ECS Meet. Abstr.*, vol. MA2020-02, no. 24, pp. 1707–1707, 2020, doi: 10.1149/ma2020-02241707mtgabs.

[4] B. Parvais *et al.*, "GaN-on-Si mm-wave RF devices integrated in a 200mm CMOS Compatible 3-Level Cu BEOL," *Tech. Dig. - Int. Electron Devices Meet. IEDM*, vol. 2020-Decem, pp. 8.1.1-8.1.4, 2020, doi: 10.1109/IEDM13553.2020.9372056.

[5] S. Yang, S. Han, K. Sheng, and K. J. Chen, "Dynamic on-resistance in GaN power devices: mechanisms, characterizations, and modeling," *IEEE J. Emerg. Sel. Top. Power Electron.*, vol. 7, no. 3, pp. 1425–1439, 2019, doi: 10.1109/JESTPE.2019.2925117.

[6] J. Kotani, M. Tajima, S. Kasai, and T. Hashizume, "Mechanism of surface conduction in the vicinity of Schottky gates on AlGaNGaN heterostructures," *Appl. Phys. Lett.*, vol. 91, no. 9, 2007, doi: 10.1063/1.2775834.

[7] W. Saito, M. Kuraguchi, Y. Takada, K. Tsuda, I. Omura, and T. Ogura, "Influence of surface defect charge at AlGaN-GaN-HEMT upon Schottky gate leakage current and breakdown voltage," *IEEE Trans. Electron Devices*, vol. 52, no. 2, pp. 159–164, 2005, doi: 10.1109/TED.2004.842710.

[8] B. M. Green, K. K. Chu, E. M. Chumbes, J. A. Smart, J. R. Shealy, and L. F. Eastman, "Effect of surface passivation on the microwave characteristics of undoped AlGaN/GaN HEMT's," *IEEE Electron Device Lett.*, vol. 21, no. 6, pp. 268–270, 2000, doi: 10.1109/55.843146.

[9] Z. H. Liu, G. I. Ng, H. Zhou, S. Arulkumaran, and Y. K. T. Maung, "Reduced surface leakage current and trapping effects in AlGaN/GaN high electron mobility transistors on silicon with SiN/Al2O3 passivation," *Appl. Phys. Lett.*, vol. 98, no. 11, pp. 1–4, 2011, doi: 10.1063/1.3567927.

[10] S. Huang, Q. Jiang, S. Yang, C. Zhou, and K. J. Chen, "Effective passivation of AlGaN/GaN HEMTs by ALD-grown AlN thin film," *IEEE Electron Device Lett.*, vol. 33, no. 4, pp. 516–518, 2012, doi: 10.1109/LED.2012.2185921.

[11] J. P. Ibbetson, P. T. Fini, K. D. Ness, S. P. DenBaars, J. S. Speck, and U. K. Mishra, "Polarization effects, surface states, and the source of electrons in AlGaN/GaN heterostructure field effect transistors," *Appl. Phys. Lett.*, vol. 77, no. 2, pp. 250–252, 2000.

[12] M. Higashiwaki, S. Chowdhury, M. S. Miao, B. L. Swenson, C. G. Van De Walle, and U. K. Mishra, "Distribution of donor states on etched surface of AlGaN/GaN heterostructures," *J. Appl. Phys.*, vol. 108, no. 6, 2010, doi: 10.1063/1.3481412.

[13] L. Gordon, M. S. Miao, S. Chowdhury, M. Higashiwaki, U. K. Mishra, and C. G. Van De Walle, "Distributed surface donor states and the two-dimensional electron gas at AlGaN/GaN heterojunctions," *J. Phys. D. Appl. Phys.*, vol. 43, no. 50, 2010, doi: 10.1088/0022-3727/43/50/505501.

[14] N. Goyal and T. A. Fjeldly, "Surface donor states distribution post SiN passivation of AlGaN/GaN heterostructures," *Appl. Phys. Lett.*, vol. 105, no. 3, pp. 1–5, 2014, doi: 10.1063/1.4891499.

[15] N. Goyal and T. A. Fjeldly, "Analytical modeling of AlGaN/AlN/GaN heterostructures including effects of distributed surface donor states," *Appl. Phys. Lett.*, vol. 105, no. 2, 2014, doi: 10.1063/1.4890469.

[16] N. Goyal and T. A. Fjeldly, "Determination of surface donor states properties and modeling of InAlN/AlN/GaN heterostructures," *IEEE Trans. Electron Devices*, vol. 63, no. 2, pp. 881–885, 2016, doi: 10.1109/TED.2015.2510427.

[17] W. Jiao *et al.*, "The characteristics of MBE-grown InxAl1-xN/GaN surface states," *Appl. Phys. Lett.*, vol. 109, no. 8, 2016, doi:

10.1063/1.4961583.
[18] M. Zhao, “Method for forming a semiconductor structure for a gallium nitride channel device,” US10991577B2, 2019.
[19] M. Zhao *et al.*, “Growth and characterization of DH-HEMT structures with various AlGaN barriers and AlN interlayers on 200 mm Si(111) substrates,” *Phys. Status Solidi Curr. Top. Solid State Phys.*, vol. 11, no. 3–4, pp. 446–449, 2014, doi: 10.1002/pssc.201300478.
[20] H. Wang, P. C. Hsu, M. Zhao, E. Simoen, A. Sibaja-Hernandez, and J. Wang, “Investigation of defect characteristics and carrier transport mechanisms in GaN layers with different carbon doping concentration,” *IEEE Trans. Electron Devices*, vol. 67, no. 11, pp. 4827–4833, 2020, doi: 10.1109/TED.2020.3025261.
[21] U. Peralagu *et al.*, “CMOS-compatible GaN-based devices on 200mm-Si for RF applications: integration and performance,” in *International Electron Devices Meeting, IEDM*, 2019, pp. 398–401, doi: 10.1109/IEDM19573.2019.8993582.
[22] J. Derluyn *et al.*, “Improvement of AlGaNGaN high electron mobility transistor structures by in situ deposition of a Si3N4 surface layer,” *J. Appl. Phys.*, vol. 98, no. 5, pp. 054501-1-054501–5, 2005, doi: 10.1063/1.2008388.
[23] S. C. Sun and J. D. Plummer, “Electron mobility in inversion and accumulation layers on thermally oxidized silicon surfaces,” *IEEE J. Solid-State Circuits*, vol. 15, no. 4, pp. 562–573, 1980, doi: 10.1109/JSSC.1980.1051439.
[24] L. Shen *et al.*, “AlGaN/AlN/GaN high-power microwave HEMT,” *IEEE Electron Device Lett.*, vol. 22, no. 10, pp. 457–459, 2001, doi: 10.1109/55.954910.
[25] C. E. Dreyer, A. Janotti, and C. G. Van De Walle, “Brittle fracture toughnesses of GaN and AlN from first-principles surface-energy calculations,” *Appl. Phys. Lett.*, vol. 106, no. 21, 2015, doi: 10.1063/1.4921855.
[26] C. E. Dreyer, A. Janotti, C. G. Van de Walle, and D. Vanderbilt, “Correct implementation of polarization constants in wurtzite materials and impact on III-nitrides,” *Phys. Rev. X*, vol. 6, no. 2, pp. 1–11, 2016, doi: 10.1103/PhysRevX.6.021038.
[27] O. Ambacher *et al.*, “Pyroelectric properties of Al(In)GaN/GaN hetero- and quantum well structures,” *J. Phys. Condens. Matter*, vol. 14, no. 13, pp. 3399–3434, 2002, doi: 10.1088/0953-8984/14/13/302.
[28] J. H. Davies, *The physics of low-dimensional semiconductors: an intorduction*. Cambridge University Press, 1998.
[29] Y. Cao, “Study of two-dimensional electron gases wave function in double-heterojunction transistors,” *Electron. Lett.*, vol. 51, no. 15, pp. 1205–1207, 2015, doi: 10.1049/el.2015.1282.
[30] I. H. Tan, G. L. Snider, L. D. Chang, and E. L. Hu, “A self-consistent solution of Schrödinger-Poisson equations using a nonuniform mesh,” *J. Appl. Phys.*, vol. 68, no. 8, pp. 4071–4076, 1990, doi: 10.1063/1.346245.
[31] S. P. Grabowski *et al.*, “Electron affinity of AlxGa1-xN(0001) surfaces,” *Appl. Phys. Lett.*, vol. 78, no. 17, pp. 2503–2505, 2001, doi: 10.1063/1.1367275.
[32] S. Khandelwal, N. Goyal, and T. A. Fjeldly, “A physics-based analytical model for 2DEG charge density in AlGaN/GaN HEMT devices,” *IEEE Trans. Electron Devices*, vol. 58, no. 10, pp. 3622–3625, 2011, doi: 10.1109/TED.2011.2161314.
[33] M. Higashiwaki, S. Chowdhury, B. L. Swenson, and U. K. Mishra, “Effects of oxidation on surface chemical states and barrier height of AlGaN/GaN heterostructures,” *Appl. Phys. Lett.*, vol. 97, no. 22, pp. 10–13, 2010, doi: 10.1063/1.3522649.
[34] M. J. Tadjer *et al.*, “Electrical and optical characterization of AlGaN/GaN HEMTs with in situ and ex situ deposited SiNx layers,” *J. Electron. Mater.*, vol. 39, no. 11, pp. 2452–2458, 2010, doi: 10.1007/s11664-010-1343-9.

confidential